Journal of Power Sources 195 (2010) 6825–6830

Contents lists available at ScienceDirect

Journal of Power Sources

journal homepage: www.elsevier.com/locate/jpowsour

Elastic softening of amorphous and crystalline Li–Si Phases with increasing Li concentration: A first-principles study

V.B. Shenoy [a,*], P. Johari [a], Y. Qi [b]

[a] Division of Engineering, Brown University, 182 Hope Street, Providence RI 02912, USA
[b] General Motors Global R&D Center, Warren, MI 48090, USA

ARTICLE INFO

Article history:
Received 2 April 2010
Received in revised form 13 April 2010
Accepted 14 April 2010
Available online 20 April 2010

Keywords:
Battery
Silicon
Lithium
Elastic constants
Amorphous alloys
Density functional theory

ABSTRACT

Knowledge of the elastic properties of Li–Si alloys as a function of Li concentration is crucial in the development of reliable deformation and fracture mechanics models for Si anodes in Li-ion batteries. Here, we have studied these properties using first-principles calculations for both amorphous and crystalline phases observed during lithiation of Si anodes. In the case of crystalline alloys, we present the anisotropic elastic tensors as well as the homogenized Young's, shear, and bulk moduli and the Poisson's ratios. We find that while these moduli decrease in an approximately linear manner with increasing Li concentration leading to significant elastic softening (by about one order of magnitude) in both crystalline and amorphous systems, the Poisson's ratios remain in the range of 0.05–0.20 and 0.20–0.30 in the case of crystalline and amorphous systems, respectively. Further, for a given Li concentration, we find that the amorphous structures are elastically somewhat softer than their crystalline counterparts, the difference being more significant (about 30–40%) in Li-poor phases. Our results underscore the importance of including the concentration dependence of elastic constants in the analysis of stress and deformation fields during lithiation and de-lithiation of Si anodes.

1. Introduction

Advanced energy storage technologies for transportation industries require further improvement of the power, energy density, and durability of Li-ion batteries for use in hybrid electric vehicles (HEV), plug-in HEV (PHEV), and all-electric vehicles (EV). Currently, the negative electrode material used in most Li-ion batteries is graphite, which forms lithium–graphite intercalation compounds (Li-GIC) [1,2]. Compared to graphite, Si can store ~10 times more Li, as the gravimetric energy densities are 3572 mAh g^{-1} for Si, and 372 mAh g^{-1} for graphite. However, this extremely high capacity of Si is associated with massive structural changes and volume expansion on the order of 300% [3–5], resulting in electrode particle fracture, disconnection between the particles, capacity loss, and thus very limited cycle life.

Wolfenstine [6] demonstrated that using the Young's modulus, the fracture toughness, and the volume change, a critical particle size for low capacity fade could be estimated with analytical modeling. Mathematical models of deformation and corresponding stress fields during lithiation and de-lithiation of idealized electrodes have been recently developed [7–14]. In all of these continuum-level models, the intrinsic mechanical properties of electrodes, such as Young's modulus and Poisson's ratio are assumed to be constants, independent of Li concentration. This is not surprising, given the lack of experimental data as well as theoretical calculations. Recently, Qi et al. used density functional theory (DFT) to demonstrate that the polycrystalline Young's modulus (E) of graphite increases linearly with Li concentration, and triples when graphite is fully lithiated to LiC_6 [15]. The lithiation process of Si is different from the interaction process of Li in graphite, where Li ions are intercalated between the graphite sheets during the charging cycle and removed during discharge with minimal structural change and a 10% variation in volume. Si experiences large structural changes upon lithiation and de-lithiation. If Si is lithiated at high temperature (415 °C) in a LiCl–KCl melt, crystalline structures of Li_7Si_3, $Li_{12}Si_7$, $Li_{13}Si_4$, and $Li_{22}Si_5$ phases will form; these structures can also be found in the equilibrium phase diagram prepared metallurgically [16]. At room temperature, in a Li-ion battery cell, when Li–Si is electrochemically cycled, crystalline Si becomes amorphous Li_xSi as it is lithiated [17]. If Si is lithiated completely, the crystalline $Li_{15}Si_4$ phase is obtained [18–19]. Using an in situ stress measurement technique, rapid rise in compressive stress has very recently been observed during lithiation of Si anodes ultimately leading to plastic flow [20]. However, data on the elastic properties and failure of Li–Si alloys is currently not available to quantitatively model these measurements.

* Corresponding author. Tel.: +1 401 863 1475; fax: +1 401 863 9009.
E-mail address: Vivek_Shenoy@brown.edu (V.B. Shenoy).

0378-7753/$ – see front matter © 2010 Elsevier B.V. All rights reserved.
doi:10.1016/j.jpowsour.2010.04.044

Table 1
Equilibrium structural parameters for Li, Si, and Li_xSi alloys obtained from PAW-GGA calculations. The number of irreducible k points used in the DFT calculations in each case is also given in the table.

Phase	x	Space group	a (Å)	b (Å)	c (Å)	Volume (Å^3)	k-points
Si	0.000	$Fd\bar{3}m$	5.472	5.472	5.472	163.814	20
LiSi	0.500	$I41/a$	9.357	9.357	5.746	503.071	144
$Li_{12}Si_7$	0.632	$Pnma$	8.532	19.612	14.302	2393.069	4
$Li_{13}Si_4$	0.765	$Pbam$	7.914	15.084	4.429	528.725	8
$Li_{15}Si_4$	0.789	$I4\bar{3}d$	10.595	10.595	10.595	1189.472	32
$Li_{22}Si_5$	0.815	$F23$	13.189	13.189	13.189	1622.280	88
Li	1.000	$Im\bar{3}_m$	3.442	3.442	3.442	40.796	20

Recently, the electronic structure, lattice vibrations, and the Birch-Murnaghan equation of state of crystalline phases was studied by Chevrier et al. using first-principles calculations [21,22]. However, the Young's and the shear moduli and the Poisson's ratio necessary for analyzing fracture and shear flow during lithiation were not considered in their study. Similarly, while the structures of amorphous phases have been considered, there is no information available on the elastic properties on amorphous alloys. In this article, we compute the complete elastic constants of Li–Si crystalline and amorphous phases, using first-principles calculations. Our goal is to derive a functional form of the relationship between the averaged elastic modulus and the Li concentration in the alloy, so that this information can be readily used in continuum-level models of deformation and failure. In the case of crystalline alloys, we present anisotropic elastic constant tensors as well as orientationally averaged Young's, shear, and bulk moduli and the Poisson ratios. In the case of amorphous alloys we directly compute these moduli using structures generated using ab initio molecular dynamics simulations. We find that the moduli of Li–Si alloys decrease almost linearly with Li concentration and it drops to about an order of magnitude of its original value of Si, when it is fully lithiated (in the $Li_{15}Si_4$ and $Li_{22}Si_4$ phases). The observed elastic softening is explained by considering the charge–density and atomic bonding in lithiated alloys. Our calculations also show why the amorphous alloys are generally softer than their crystalline counterparts. These results suggest that mechanical modeling of Si anode deformation and fracture needs to account for varying material and elastic properties with Li concentration.

2. Methods

DFT calculations were performed using the Vienna Ab Initio Simulation (VASP) Package [23,24] with the Projector Augmented Wave (PAW) method and the Perdew–Burke–Ernzerhof (PBE) form of the generalized gradient approximation for exchange and correlation. For crystalline phases, the structures of the alloys were obtained from crystal structure database and from experimental work [25–30]. From convergence studies, we determined the kinetic energy cutoff in the plane wave expansion to be 300 eV. The optimized lattice parameters of the crystalline Li–Si phases obtained from our calculations are summarized in Table 1. The number of irreducible k points used for each of the Li–Si alloy phases is also given in this table. The structural data in Table 1 agrees well with experimental studies and previous theoretical work [18,19,31–37].

Amorphous systems were created using ab initio molecular dynamics (MD) simulations using the VASP package. We started with a periodic super cell that consists of the alloy in its crystalline form (typically with 100–150 atoms). The cell was then heated to a temperature much larger than the melting temperature of the crystalline phase (3000–4000 K). The system was allowed to equilibrate at this temperature for 5000 MD time steps (each MD time step = 1 fs). To obtain the amorphous phase, we then cooled these structures to room temperature at the rapid rate of 200 K per 200 MD time steps, *i.e.*, we sequentially reduced the temperature by 200 K and let the system evolve for 200 MD steps. The geometries obtained at room temperature were then relaxed with an atomic force tolerance of 0.01 eV Å^{-1}. In our relaxation simulations, along with the atomic coordinates, we also allowed variations of the dimensions as well as the shape of the super cell. For a given Li composition up to five statistically independent realizations of the amorphous structures were created. We emphasize that our method for generating the amorphous structures is very different from the protocol employed in Ref. [38]. In particular, we do not rely on initial atomic configurations obtained from empirical potentials. Our method is based entirely on the DFT formalism and should therefore be more accurate. Furthermore, the method we have outlined is simple to implement as it employs well-established MD time-integration techniques. Nonetheless, we have found that our calculated formation energies for amorphous systems (*c.f.* Table 2) are in very good agreement with the results obtained by Chevrier et al. [38].

In case of crystalline systems, elastic constants were determined by computing the energies of deformed unit cells. For cubic type phases, Si, $Li_{15}Si_4$, and Li, distortions with tetragonal and orthorhombic shear, and isotropic distortion along the three lattice vectors were applied to obtain three independent elastic constants C_{11}, C_{12}, and C_{44} (all elastic constants are expressed using the Voigt notations [39]). For the tetragonal Li–Si phase, we applied six different deformation modes to compute C_{11}, C_{12}, C_{13}, C_{33}, C_{44}, and C_{66}. For $Li_{12}Si_7$ and $Li_{13}Si_4$, expansion along three high-symmetry directions, three monoclinic distortions, and three orthorhombic distortions were applied to obtain nine independent elastic constants. We allowed relaxation of the atomic positions in all the strained supercells.

Next, we discuss the methodology used to compute the elastic constants of amorphous alloys. Since amorphous phases are isotropic and are therefore characterized by two independent elastic constants, the bulk modulus B and the modulus C_{11}. We first computed B and C_{11} and once these quantities were known, we used the relations between different elastic constants [39] to deduce the Young's modulus, the shear modulus, and the Poisson's ratio. Note that the basis vectors of the optimized amorphous supercell obtained using our relaxation procedure need not in

Table 2
Comparison of the calculated formation energies with the work of Chevrier et al. [38] for amorphous Li–Si phases. The formation energy was calculated using expression: $E_f = E(Li_xSi) - [xE(Li) + E(Si)]$, where x is the number of Li atoms per Si atoms, $E(Li_xSi)$ is the total energy of the Li_xSi structure divided by the number of Si atoms used in the calculation, E(Li) is the total energy of the single Li atom elemental BCC Li (−1.895 eV), and E(Si) is the total energy of a single Si atom in elemental Si diamond lattice (−5.422 eV).

Phase (x in Li_xSi)	Formation energy E_f (eV)	
	Our results	Chevrier et al. [38]
a-LiSi (x = 1)	−0.20	−0.22
a-$Li_{12}Si_7$ (x = 1.7)	−0.40	−0.44
a-$Li_{15}Si_4$ (x = 3.75)	−0.88	−0.80

Table 3
Calculated elastic constants C_{ij} (in Voigt notation), for Li, Si and Li–Si alloys. All quantities are in units of GPa.

Phase	C_{11}	C_{22}	C_{33}	C_{12}	C_{13}	C_{23}	C_{44}	C_{55}	C_{66}
Si	152.168	152.168	152.168	56.842	56.842	56.842	75.034	75.034	75.034
LiSi	101.160	101.160	74.506	20.645	37.343	37.343	55.435	55.435	36.000
$Li_{12}Si_7$	92.500	95.905	88.837	4.987	11.403	8.801	30.168	34.681	44.939
$Li_{13}Si_4$	77.207	64.702	82.247	18.503	7.412	6.746	73.637	32.866	40.595
$Li_{15}Si_4$	46.644	46.644	46.644	21.907	21.907	21.907	28.019	28.019	28.019
$Li_{22}Si_5$	89.847	89.847	89.847	1.740	1.740	1.740	30.954	30.954	30.954
Li	17.952	17.952	17.952	8.936	8.936	8.936	12.423	12.423	12.423

general be orthogonal to each other. Therefore, we employed the following procedure to obtain the elastic constants. Using A_i to denote the basis vectors of the cell, we applied the deformation gradient ξ,

$$\xi = \begin{bmatrix} 1+\varepsilon & 0 & 0 \\ 0 & 1+\varepsilon & 0 \\ 0 & 0 & 1+\varepsilon \end{bmatrix}$$

to the basis vectors to obtain the deformed lattice vectors $\xi(\varepsilon)A_i$. Here, ε is the percentage deformation/strain. The relaxed energy of the deformed cell was then computed and fitted to the equation $E(\varepsilon) = E_0 + c\varepsilon^2$, where E_0 is the energy of the undeformed cell. The bulk modulus can then be calculated using formula:

$$B = \frac{2c}{9V_0} \tag{1}$$

where V_0 is the volume of the unstrained cell and c is the coefficient of ε^2 in the quadratic fit.

To calculate elastic constant C_{11}, average of components of C_{11} along three orthogonal axes was taken. C_{11} along the global x-axis (C_{11}^x) of the cell was calculated by multiplying the vectors of the unit cell with the deformation matrix ξ', which was given as:

$$\xi' = \begin{bmatrix} 1+\varepsilon & 0 & 0 \\ 0 & 1 & 0 \\ 0 & 0 & 1 \end{bmatrix}.$$

Similarly, C_{11}^y and C_{11}^z were calculated using the deformation matrix in which $1+\varepsilon$ was shifted to 22 and 33 positions of the matrix given above, respectively. For a truly isotropic system these constants should all be equal. In our calculations we found only small differences (about 10%) between these cases, confirming that our procedure for creating amorphous structure does indeed lead to a nearly isotropic structure. As in the case of bulk modulus, the computed energies of the deformed configurations were fit to the expression $E(\varepsilon) = E_0 + d\varepsilon^2$. The elastic constant C_{11} was then obtained using the volume of the unstrained cell and the coefficient of ε^2 from the formula:

$$C_{11} = \frac{2d}{V_0}. \tag{2}$$

Using the computed values for B and C_{11}, the shear modulus G, Young's modulus E, Poisson's ratio ϑ, for all the systems were then calculated using the expressions:

$$G = \frac{3(C_{11} - B)}{4} \tag{3}$$

$$E = \frac{9B(C_{11} - B)}{(C_{11} + 3B)}, \tag{4}$$

$$\vartheta = \frac{(3B - C_{11})}{(C_{11} + 3B)} \tag{5}$$

3. Results and discussion

The array of elastic constants for crystalline phases considered in our work is given in Table 3. While the elastic constants obtained from the DFT calculations are for single crystals, lithiated Si anodes usually display polycrystalline micro-structures formed out of aggregation of single crystal grains rotated relative to each other. Hence, we proceed to deduce polycrystalline properties from the computed anisotropic single crystal elastic constants. The determination of the stress or strain distribution in the assembly of a polycrystalline aggregate with respect to an external load, can be established from the continuum theories based on Voigt [40] and Reuss [41] approaches that obtain effective isotropic elastic constants by averaging the anisotropic elastic constants over all possible orientations of the grains in a polycrystal. Using energy considerations, Hill [42] proved that the Voigt and Reuss moduli represent upper and lower limits of the true polycrystalline constants, and suggested that a practical estimate of the elastic moduli was the arithmetic means of the extremes. We have therefore adopted the Hill averaging procedure in our work.

The orientation averaged elastic constants and Poisson ratios for crystalline phases are plotted in Fig. 1 along with the plots of the elastic constants for amorphous structures. These quantities are plotted with respect to the Li fraction y, of the alloy. For the alloy Li_xSi, y can be related to x, through the expression $y = x/(1+x)$. Note that while x is the ratio of the Li atoms in the alloy compared to the number of Si atoms, y is the ratio of the Li atoms to the total number of atoms. The advantage of using y in favor of x is that for elemental Li $x \to \infty$, while y is 1. Therefore all the alloy phases can be explored by letting y vary between 0 (Si) and 1 (Li). A further advantage of plotting the elastic moduli with respect to the Li fraction y is that it allows us to assess the validity of the "law of mixtures", which predicts a linear dependence of the computed properties with respect to y. Therefore, in order to compare the elastic properties of alloy phases with that of pure Si and pure Li we have plotted the elastic moduli in the range $0 \le y \le 1$.

From Fig. 1, one can see that for the crystalline systems, the bulk, shear, and Young's moduli depend very strongly on Li concentration, showing significant softening in the Li-rich phases. These moduli for the most lithiated phases, $Li_{15}Si_4$ and $Li_{22}Si_4$, are smaller than the corresponding values for Si by nearly one order of magnitude. Furthermore, a linear decrease in these properties with increase in Li concentration y, provides a good approximation to our results for the bulk, Young's and shear moduli of the crystalline phases. The linear fit to the Poisson's ratio is not as reliable; the ratio fluctuates between 0.05 and 0.20. Linear fits also provide an excellent description of the elastic moduli of the amorphous phases, suggesting that the elastic constants follow the law of mixtures to a reasonable extent. Writing the moduli in the form $Ay + B(1-y)$, we have provided the best fit parameters A and B for each of the computed elastic constants for both amorphous and crystalline phases in Table 4. Using these parameters, the elastic constants of the Li_xSi alloy, one can then obtain using the expression $(Ax+B)/(1+x)$; for example, the Young's modulus for crystalline and amorphous Si can be represented as: $E(c - Li_xSi) = (37.96x + 156.13)/(1+x)$ and $E(a - Li_xSi) = (18.90x + 90.13)/(1+x)$, respectively. These expressions can readily be used to account

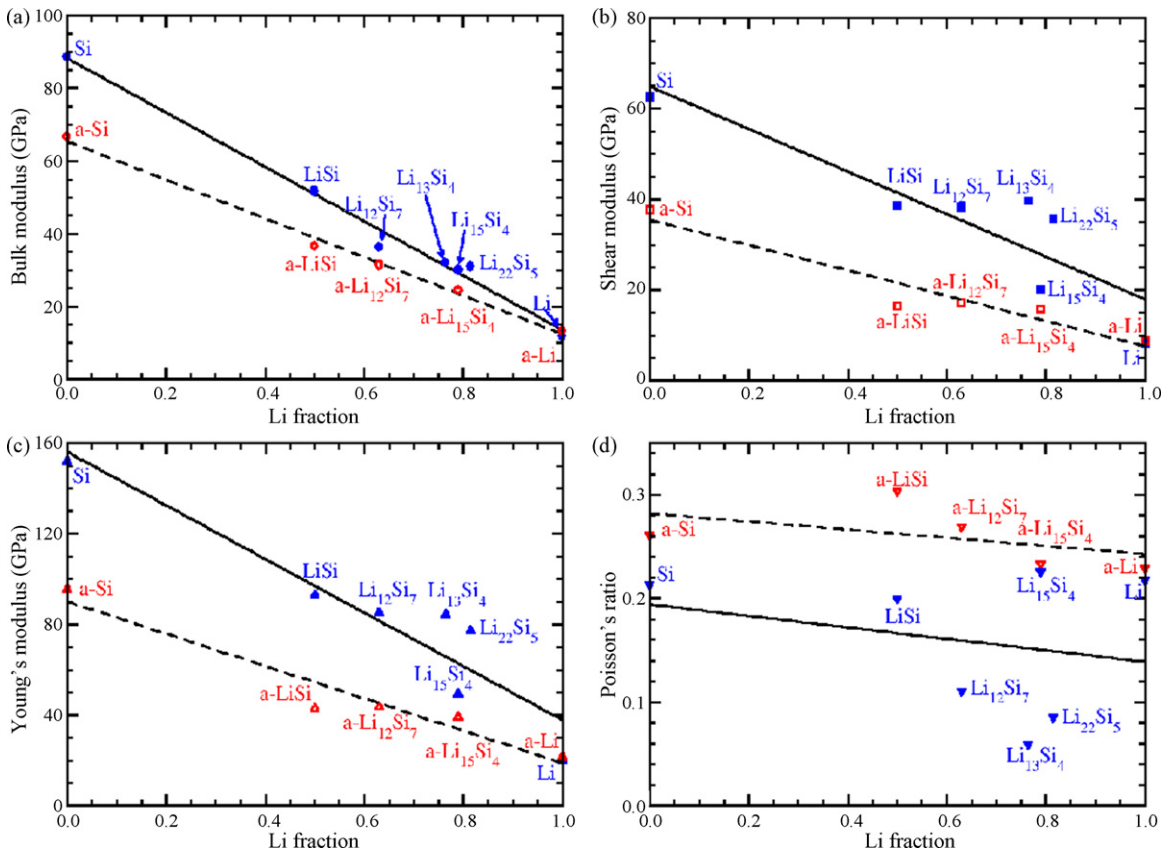

Fig. 1. (a) Bulk modulus B, (b) shear modulus G, (c) Young's modulus E, and (d) Poisson's ratio ϑ of Li–Si alloys plotted as a function of Li fraction in crystalline (solid symbols) and in amorphous (open symbols) phases for the alloy Li_xSi. The Li fraction in the alloy is given by $x/(1+x)$. Solid and broken lines show linear fits for the crystalline and the amorphous systems, respectively.

for the composition dependence of elastic constants in continuum elastic models for stress generation during lithiation. We note that the goodness of fit on the Poisson's ratio is lower compared to other elastic constants. Unlike other quantities that show large variations (close to an order of magnitude), the Poisson's ratio for both the crystalline and amorphous phases of Li and Si are close (This is evident from the values of A and B given in Table 4). Also, the Poisson's ratios of the alloys are close to values for the elemental phases but fluctuate by a small amount, between 0.3 and 0.24 for amorphous phases and between 0.23 and 0.07 for crystalline phases. Since the Poisson's ratio enters continuum models of intercalation and fracture [7–14] through factors like $1-\vartheta$ $1-2\vartheta$, and $1-\vartheta^2$, the errors that arise from using our fits would be rather small (of the order of 20%) even though the goodness of fit is not high.

Next, we compare the elastic properties of amorphous alloys with their crystalline counterparts. From the plots of the elastic moduli in Fig. 1, it is clear that the slopes of the moduli vs. composition fits in the case of amorphous systems are smaller than the slopes in the case of crystalline phases. This can be understood by noting that the moduli of amorphous Si are smaller than those of cubic Si by about 30–50%, while the moduli of amorphous Li and BCC Li are nearly equal. Indeed, the orientations of the sp^3 covalent bonds in amorphous Si can deviate considerably from the tetrahedral angle, which leads to softening of amorphous phase. Since this directional dependence of the bonds is absent in the case of metallic Li bonds, the elastic constants of a-Li are close to that of BCC Li. Subsequently, the elastic properties of Li-rich amorphous alloys are close to corresponding crystalline phases while the difference between the moduli of the crystalline and the amorphous phases is much larger in the case of Si-rich Li–Si alloys.

To further relate the computed elastic properties to electronic structure, we obtained the net charge on Si atoms for each Li_xSi alloy. As shown in Table 5 and Figs. 2 and 3, Li donates all its elec-

Table 4
Values of A and B in the expression $(Ax+B)/(1+x)$ for the elastic constants (bulk, shear, and Young's moduli and Poisson's ratio), where x refers to the concentration of Li atoms relative to the concentration of Si in the alloy Li_xSi. These constants are obtained from the linear fits of elastic constants for crystalline and amorphous systems (*c.f.* Fig. 1). Goodness of fit (R^2) is also provided in the table.

Elastic constants	Crystalline			Amorphous		
	A	B	R^2	A	B	R^2
B	13.61	88.32	0.99	12.46	65.44	0.99
G	18.01	64.91	0.79	7.63	35.51	0.92
E	37.96	156.13	0.88	18.90	90.13	0.93
ϑ	0.14	0.19	0.06	0.24	0.28	0.24

Table 5
Net charges on Li and Si atoms in Li–Si alloys. The labels of the Si atoms (1–4) are given in Figs. 2 and 3. The net charges on the atoms were computed from the charge densities obtained from the PAW-PBE calculations using the Bader charge analysis.

Phase (x in Li_xSi)	Charge on Li atoms	Charge on Si atoms			
		Si(1)	Si(2)	Si(3)	Si(4)
LiSi ($x=1$)	1.00	−1.00	–	–	–
a-LiSi ($x=1$)	1.00	−1.04	−0.40	−1.14	−0.78
$Li_{12}Si_7$ ($x=1.7$)	1.00	−2.00	−1.14	−2.43	−1.60
$Li_{13}Si_4$ ($x=3.25$)	1.00	−3.95	−2.55	–	–
$Li_{15}Si_4$ ($x=3.75$)	1.00	−3.75	–	–	–
a-$Li_{15}Si_4$ ($x=3.75$)	1.00	−4.15	−2.67	−2.90	−4.05
$Li_{22}Si_5$ ($x=4.4$)	0.91	−4.00	–	–	–

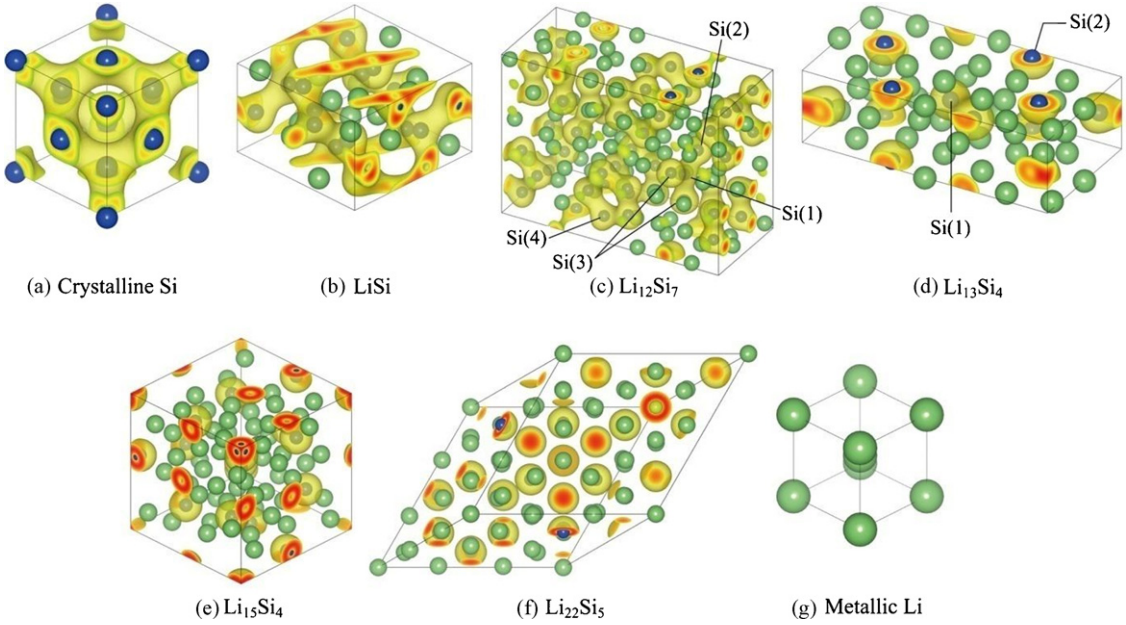

Fig. 2. Charge distribution in crystalline Li–Si alloys with charge density contour level of 0.04 e bohr^{-3}. Si and Li atoms given are represented by blue and green spheres, respectively. (For interpretation of the references to color in this figure legend, the reader is referred to the web version of the article.).

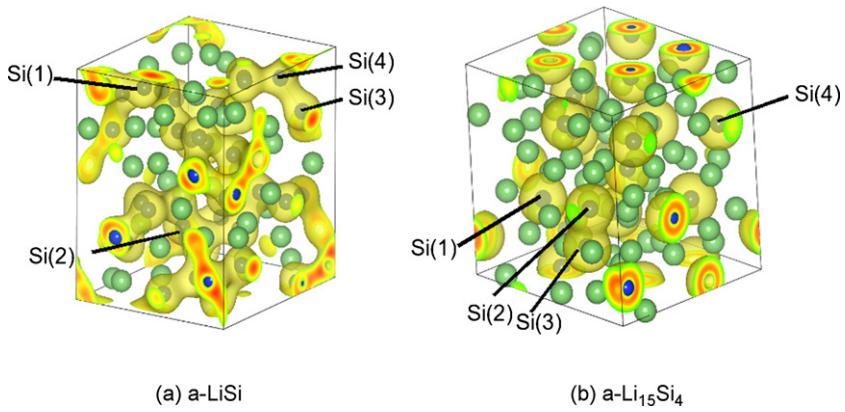

Fig. 3. Charge distribution in amorphous (a) LiSi and (b) $Li_{15}Si_4$ alloys, with charge density contour level of 0.04 e bohr^{-3}. Si and Li atoms are given represented by blue and green spheres, respectively. (For interpretation of the references to color in this figure legend, the reader is referred to the web version of the article.).

trons to Si atoms, becoming Li ion with +1 net charge. Si atoms take up — 1–4 electrons, leading to a net charge of −1 to −4 compared to the crystalline Si. The charge state of Si depends on the number of both Si and Li neighbors. In the case of $Li_{12}Si_7$ phase, Si atoms can acquire as many as 4 distinct charge states depending on where they are located in the unit cell; 4 Si atoms sitting at the center of the triangle in Fig. 2(c) are in charge state of −2, while the 4 Si atoms sitting at the top of the triangle have a net charge of −1.14 and the 8 Si atoms that form the base of the triangle acquire a charge of −2.43, while the 40 Si atoms that form pentagons possess net charge of −1.6. For the case $Li_{13}Si_4$, 4 Si atoms that form dumbbells are in a charge state of −3.95 while the 4 isolated Si atoms possess a charge of −2.55. Charge states of Si atoms in LiSi and $Li_{15}Si_4$ phases were estimated to −1 and −3.75, respectively. For amorphous structures, different Si atoms have different numbers or Li and Si neighbors, so the charge on Si atoms varies accordingly. For example, Si atoms that are not in the vicinity of other Si atoms and are surrounded by Li atoms (for example Si(1) and Si(4) in Fig. 3(b)) form ionic Li–Si bonds and possess a net charge of −4. On the other hand Si atoms in close proximity (for example Si(2) and Si(3) in Fig. 3(b)) carry only net charge in the range −2.6 to −2.9, indicating reduced ionic character.

Based on these calculations it is clear that covalent Si–Si bonds are replaced with ionic Li–Si bonds with increasing Li concentration. This can be clearly seen from the charge density plots in Fig. 2 that show the decrease in overlap of the charge densities from neighboring Si atom as one proceeds from LiSi to $Li_{22}Si_5$. Our calculations therefore show that the ionic Li–Si bonds are intermediate in strength compared to covalent Si–Si bonds and the metallic Li–Li bonds, Elastic softening of the alloy phase is consistent with the increase in the relative population of these ionic bonds.

4. Conclusions

In conclusion, we have computed the elastic properties of crystalline and amorphous Li–Si alloys and have found that they depend strongly on Li concentration. By considering the electronic structure of the alloys, we attribute elastic softening to the increase in the population of ionic Li–Si bonds that are weaker than the covalent Si–Si bonds. Since the elastic moduli at the highest levels of lithiation are smaller than that of Si by an order of magnitude, our results have important implications in the fracture and flow of Li–Si alloys. Since fracture energy scales with modulus of the alloy, we expect the fracture energy also to decrease with Li concentration.

As the level of stresses achieved during charging and discharging cycles in Li–Si alloy should depend on the modulus and fracture strength of the alloy, the composition dependence derived in this work should be included in the mathematical models for deformation and failure. As noted in Section 1, recent measurements [4,5,20,31] show that stress contributes significantly to chemical potential of lithiated Si and hence the electrode potential. Our work should provide a quantitative framework for analyzing these and future measurements on stress evolution during amorphization of lithiated Si electrodes.

Acknowledgments

The research support of the NSF through grants CMMI- 0855853, DMS- 0854919 and DMS- 0914648 and the GM-Brown collaborative research laboratory is gratefully acknowledged. Computational support for this research was provided by the grant TG-DMR090098 from the TeraGrid advanced support program and the Center for Computation and Visualization at Brown University. We thank Pradeep Guduru, Sang-Pil Kim, and Mark Vurbrugge for useful discussions and suggestions.

References

[1] R.A. Huggins, Advanced Batteries—Materials Science Aspects, Springer, 2009.
[2] J.R. Dahn, Phys. Rev. B 44 (1991) 9170–9177.
[3] L.Y. Beaulieu, T.D. Hatchard, A. Bonakdarpour, M.D. Fleischauer, J.R. Dahn, J. Electrochem. Soc. 150 (2003) A1457–A1464.
[4] S.-J. Lee, J.-K. Lee, S.-H. Chung, H.-Y. Lee, S.-M. Lee, H.-K. Baik, J. Power Sources 97–98 (2001) 191–193.
[5] W. Wang, P.N. Kumta, J. Power Sources 172 (2007) 650–658.
[6] J. Wolfenstine, Mater. Lett. 57 (2003) 3983–3986.
[7] Y.-T. Cheng, M.W. Verbrugge, J. Power Sources 190 (2009) 453–460.
[8] R.A. Huggins, W.D. Nix, Ionics 6 (2000) 57–63.
[9] J. Christensen, J. Newman, J. Electrochem. Soc. 153 (2006) A1019–A1030.
[10] J. Christensen, J. Newman, J. Solid State Electrochem. 10 (2006) 293–319.
[11] X. Zhang, W. Shyy, A.M. Sastry, J. Electrochem. Soc. 154 (2007) A910–A916.
[12] X. Zhang, A.M. Sastry, W. Shyy, J. Electrochem. Soc. 155 (2008) A542–A552.
[13] Y.-T. Cheng, M.W. Verbrugge, J. Appl. Phys. 104 (2008) 083521.
[14] M.W. Verbrugge, Y.-T. Cheng, Electrochem. Soc. Trans. 16 (2008) 127–139.
[15] Y. Qi, H. Guo, L.G. Hector Jr., A. Timmons, J. Electrochem. Soc. 157 (2010) A558–A566.
[16] C.J. Wen, R.A. Huggins, J. Solid State Chem. 37 (1981) 271–278.
[17] P. Limthongkul, Y.-I. Jang, N.J. Dudney, Y.-M. Chiang, Acta Mater. 51 (2003) 1103–1113.
[18] M.N. Obrovac, L. Christensen, Electrochem. Solid-State Lett. 7 (2004) A93–A96.
[19] J. Li, J.R. Dahn, J. Electrochem. Soc 154 (2007) A156–A161.
[20] V.A. Sethuraman, M.J. Chon, M. Shimshal, V. Srinivasan, P.R. Guduru, J. Power Sources 195 (2010) 5062–5066.
[21] V.L. Chevrier, J.W. Zwanziger, J.R. Dahn, J. Alloys Comp. 496 (2010) 25–36.
[22] V.L. Chevrier, J.W. Zwanziger, J.R. Dahn, Can. J. Phys. 87 (2009) 625–632.
[23] G. Kresse, J. Furthmüller, Phys. Rev. B 54 (1996) 11169–11186.
[24] G. Kresse, J. Furthmüller, Comput. Mater. Sci. 6 (1996) 15–50.
[25] H. Axel, H. Schäfer, A. Weiss, Z. Naturforsch. B: Chem. Sci. 21B (1966) 115–117.
[26] R.W.G. Wyckoff, Crystal Structures, second ed., Robert E. Krieger, Malabar, Florida, USA, 1963.
[27] R. Nesper, H.G. von Schnering, J. Curda, Chem. Ber. 119 (1986) 3576–3590.
[28] H.G. Von Schnering, R. Nesper, K.-F. Tebbe, J. Curda, Z. Metallk. 71 (1980) 357–363.
[29] I. Barvik, Czech. J. Phys. B 33 (1983) 1338–1346.
[30] U. Frank, W. Müller, H. Schäfer, Z. Naturforsch. B: Chem. Sci. 30B (1975) 10–13.
[31] B. Key, R. Bhattacharyya, M. Morcrette, V. Seznéc, J.-M. Tarascon, C.P. Grey, J. Am. Chem. Soc. 131 (2009) 9239–9249.
[32] H.G. von Schnering, R. Nesper, J. Curda, K.-F. Tebbe, Angew. Chem. Int. Ed. Engl. 19 (1980) 1033–1034.
[33] J. Evers, G. Oehlinger, G. Sextl, Angew. Chem. Int. Ed. Engl. 32 (1980) 1442–1444.
[34] T.D. Hatchard, J.R. Dahn, J. Electrochem. Soc. 151 (2004) A838–A842.
[35] Y. Kubota, M.C.S. Escano, H. Nakanishi, H. Kasai, J. Alloys Compd. 458 (2008) 151–157.
[36] Y. Kubota, M.C.S. Escano, H. Nakanishi, H. Kasai, J. Appl. Phys. 102 (2007) 053704.
[37] H. van Leuken, G.A. de Wijs, W. van der Lugt, Phys. Rev. B 53 (1996) 10599–10604.
[38] V.L. Chevrier, J.R. Dahn, J. Electrochem. Soc. 156 (2009) A454–A458.
[39] L.D. Landau, E.M. Lifshitz, Theory of Elasticity, third ed., Butterworth-Heinemann, Oxford, 1999.
[40] W. Voigt, Lehrbuch der Kristallphysik, Taubner, Leipzig (1928) 830–831.
[41] A. Reuss, Z. Angew. Math. Mech. 9 (1929) 49–58.
[42] R. Hill, Proc. Phys. Soc. Lond. 65 (1952) 349–354.